気象庁欧文海洋報告

第35巻 第1-2号

THE OCEANOGRAPHICAL MAGAZINE

Vol. 35 Nos. 1-2

LIBRARY
AUG 30 1985
National Marine Fisheries Service
2570 Dole Street
Honolulu, Hawaii

CONTENTS

TAKEUCHI, M. and M. TAKADA: Development of the Operational Wave Forecast Model in Coastal Area 1

SHIBATA, A. and I. EGUCHI: Frontal Eddies Observed in the East China Sea in May and October of 1982..... 21

Note

NAGASAKA, K., M. SAIKI and T. ANDOW: On a free fall and retrieval method for a small CTD 31

Published by the Japan Meteorological Agency

March, 1985

投稿規定

1　資　格

原則として，気象庁職員に限る。ただし，気象庁職員との連名の場合は，この限りでない。

2　論文及び報文（以下「論文等」という。）の内容

未発表の原稿で，海洋（物理・化学・生物・地質など）及び海上気象（波浪・海氷・海気相互関係など）に関する論文並びに気象庁における海洋・海上気象業務の活動，そのために開発された測器及び方法に関する報文など。

3　書き方

(1) 用語は，欧文（原則として英文）とする。

(2) 論文等には，英文（300語以内）及び和文（800字以内）の要約を付ける。要約は，方法・測器・実験・観測の結果・仮定・理論などの中味が読みとれるように留意し，なるべく指定の長さで簡潔に書く。

(3) 論文等の始めには，題名・著者名及所属機関名を明記する。和文の要約にも同様のことを明記する。

(4) 原稿は，厚手の用紙にダブルスペースでタイプする。

(5) 図は，白紙又は青方眼紙に墨入れし，図及び図中の文字の大きさは，印刷の際の縮小率を考えて作成する。特に重要な図は，投稿者が大きさを指定する（印刷の都合上，希望どおりにならないこともある。）

(6) 図（写真を含む。）及び表には，必ず説明を付ける。図の説明文は，別紙にタイプする。折り込みの図及び表は，なるべく避ける。図及び表のそう入箇所を本文の欄外に記入する。

(7) 数式は，2行取りに書き，数式の文字及び記号をはっきりと説明する。

(8) 論文等の中に文献を引用する場合は，「ALLEN (1927)」又は「(ALLEN, 1927)」のように書く。

(9) 引用文献は，最後にまとめて付け，著者名のアルファベット順に並べる。書き方は次のようにする。

ALLEN, W.E. (1927): Surface catches of marine diatoms and dinoflagellates made by U.S.A. Pioneer in Alaskan waters in 1923. *Bull. Scripps Inst. Occanogr., Tech. Ser.* **1**(4), 39–48.

BUDYKO, M. I. (1956): *The heat balance of the earth's surface.* Hydrometeorological Publishing House, Leningrad, pp. 254.

VERONINS, G. and H. STOMMEL (1956): The action of a variable wind stress on a stratified ocean. *J. Mar. Res.*, **15**(1), 43–75.

4　提出方法

投稿票を付け，本稿のほかにコピー（図及び表を含む。）2部を添える。

5　送付先

気象庁海洋気象部海洋課

6　その他

論文等1編につき別刷り50部を著者に無料で送付する。

Oceanographical Magazine

編集委員長　Editor

斎　藤　　実，M. SAITO

編集委員　Editorial Board

赤　川　正　臣，M. AKAGAWA**
荒　川　正　一，S. ARAKAWA*
磯　崎　一　郎，I. ISOZAKI**
窪　田　　将，M. KUBOTA***
長　坂　昂　一，K. NAGASAKA*
鷺　　猛，T. SAGI*
佐　野　　昭，A. SANO*
周　東　健　三，K. SHUTO*
杉　村　行　勇，Y. SUGIMURA**

* 気　象　庁　JAPAN METEOROLOGICAL AGENCY

** 気象研究所　METEOROLOGICAL RESEARCH INSTITUTE

*** 気象大学校　METEOROLOGICAL COLLEGE

The Oceanographical Magazine
Vol. 35, Nos, 1-2, pp. 1 to 20, March 1985

Development of the Operational Wave Forecast Model in Coastal Area

Masaaki TAKEUCHI and Masayuki TAKADA

Japan Meteorological Agency

(Received October 1, 1984; Accepted December 12, 1984)

Abstract: This paper describes a numerical prediction model developed for the operational coastal wave forecast.

An ocean wave model was already developed based on the linear spectral concept by I. Isozaki and T. Uji in 1973 and has been used successfully in the North Pacific wave forecast since March 1977 in the Japan Meteorological Agency, Tokyo (JMA). Succeedingly, a coastal wave forecast model was developed and has been used for operational work since March 1983. The model consists of coarse mesh wave model (381 km spacing between adjacent grids), fine mesh wave model (127 km) and coastal wave model (10 km). The first two models are similar to the previous ocean wave model. In the coastal wave model, wind waves and swell are calculated independently and combined to make wave information at every grid point in coastal areas.

Wind wave and swell calculated by means of the significant wave method and spectral method respectively. Post analysis rerealed that the results of the model prediction technique agrees fairly well with the actual observations. The coastal wave information is now broadcast by land-line facsimile as two charts, one is the analysis chart and the other the 24 hours prognostic chart.

1. Introduction

Disasters at sea have been caused by innumerably different severe meteorological and marine situations. These disasters still continue to occur in spite of our increased knowledge about the sea state.

Accordingly, accurate and precise sea surface information, supplied routinely, is badly needed for the safety and economic efficiency of the marine industry.

In the JMA, the ocean wave information service covering the western North Pacific was started in 1972. At that time manual analysis of actual sea conditions making use of meteorological and maritime reports from ships was carried out and was broadcast by radio facsimiles as the ocean wave analysis chart covering the western North Pacific.

In 1977, numerical prediction model of ocean wave conditions was introduced, and an ocean wave forecast chart covering the same region as in the analysis chart was broadcast by radio facsimile.

These two charts are broadcast once a day continuously since 1977.

Recently economic activity has increased in the coastal region and requests for wave forecasts in the region have gradually risen. These requests have originated from a wide variety of organizations involved with ocean development, ships operating in the coastal areas, fisheries and tourist organizations.

We, in collaboration with the Meteorological Research Institute (MRI), have developed a coastal wave model. The calculated products by the model are translated into coastal wave chart and two kinds of information (Analysis and Forecast) are broadcast every day since March 1983 using land-line communication system.

In this report we introduce an outline of the ocean wave model, the coastal wave model, the operational procedures of the model and an evaluation of the performance using real time data. ("Wind wave" is used here as a general term for waves which are growing under a local wind. "Wave" means both of wind wave and swell.)

2. Ocean wave model

An ocean wave model was developed by ISOZAKI and UJI (1973, 1974) and has been operationally used by the JMA for wave forecast. The model consisted of two parts, a numerical model of marine surface winds which is established by using an operational numerical weather forecast system, and a numerical model of ocean waves by means of the known relationships between winds and waves.

2.1 Numerical model of marine surface winds

To know the surface wind field is very important because of its significant influence on the change of sea conditions. The field is now inferred mainly by surface wind reports from merchant ships.

Accordingly, vast data scarce areas exist over the ocean because of the limited distribution of ship routes. Many investigations have verified the usefulness of satellite derived low level wind data but these data are not yet used operationally.

It is necessary to obtain marine surface winds over the analysis area before carrying out the numerical wave analysis and wave forecast. BLACKADAR (1965) and CARDONE (1969) proposed a method of marine surface wind estimation. ISOZAKI and UJI (1974) used this method and constructed a computation scheme for the routine wave operations of the JMA. It is a two layer baroclinic non-neutral method and produces surface winds and friction velocities. As seen in Fig. 1, the atmospheric surface boundary layer is assumed

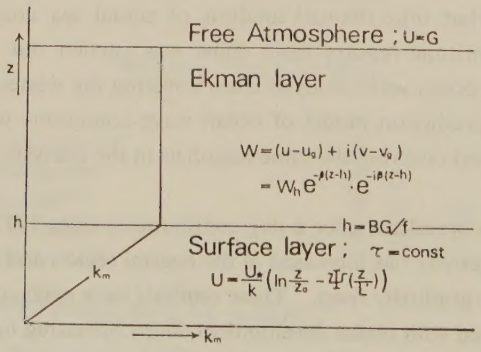

Fig. 1. Model of atmospheric boundary layer.

to be separated into two regions: the surface layer and the Ekman layer. In the surface layer, the Coriolis parameter is neglected, the turbulent transfer coefficient for momentum (K_m) increase almost linearly with height, and the wind stress is constant. The vertical wind profile is as follows;

$$U_z=\frac{u_*}{k}\left[\ln\frac{z}{z_0}-\phi\left(\frac{z}{L'}\right)\right] \tag{2.1}$$

where U_z is the wind speed at the height z, u_* the friction velocity, k the Karman constant, z_0 the roughness parameter, L' the modified Monin-Obukhov's stability length, and $\phi(z/L')$ the correction term with respect to the atmospheric stability.

The height of the surface layer h is given by Blackadar's formulation;

$$h=B_0G/f \tag{2.2}$$

where B_0 is the constant, G the gradient wind, and f the Coriolis parameter.

It is assumed in the Ekman layer that K_m is constant, the wind stress decreases with height and the vertical wind distribution is assumed to be specified by Ekman's solution. We represent the components of $\vec{U}$ and $\vec{G}$ as (u, v) and (u_g, v_g) respectively, and the deviation of $\vec{U}$ from $\vec{G}$ as follows;

$$\vec{W}=(u-u_g)+\mathrm{i}(v-v_g) \tag{2.3}$$

then the solution is

$$\vec{W}=W_h\mathrm{e}^{-\beta(z-h)}\mathrm{e}^{\mathrm{i}\beta(z-h)} \tag{2.4}$$

where W_h is the W at the height h, and;

$$\beta=\sqrt{f/2K_m} \tag{2.5}$$

We assume boundary condition as follows;

$$\left.\begin{aligned}&\vec{U}=0 \qquad \text{at} \quad z=z_0\\&\vec{U}=\vec{G} \qquad \text{at} \quad z=\infty\\&\vec{U},\ \frac{\partial\vec{U}}{\partial z},\ \vec{\tau} \quad \text{are continuous through } z=h\end{aligned}\right\} \tag{2.6}$$

where $\vec{U}$, $\vec{G}$ and $\vec{\tau}$ are the vectors of wind, gradient wind and wind stress respectively and these are represented by complex variable form.

Using these results, Equation (2.1) can describe completely the profile of the wind in the surface layer.

2.2 Numerical model of ocean waves

The numerical computation of wave conditions is performed by means of a spectral wave model developed by ISOZAKI and UJI (1973). The model is based on the two-dimensional spectral concept of ocean waves and contains five energy transfer processes. These are the linear and exponential wave growths, wave breaking, frictional dissipation and the effect of opposing winds.

The fundamental equations are represented as follows according to the each stage of the sea state.

$$\left.\begin{aligned}
&\frac{\partial S}{\partial t}=-C_g\cdot\nabla S+(A+BS)\left\{1-\left(\frac{S}{S_\infty}\right)^2\right\}\Gamma(\theta') && \theta'\leq 90^\circ,\ S\leq S_\infty\\
&\frac{\partial S}{\partial t}=-C_g\cdot\nabla S-Df^4S && \theta'\leq 90^\circ,\ S>S_\infty\\
&\frac{\partial S}{\partial t}=-C_g\cdot\nabla S-\{B\Gamma(\theta')+Df^4\}S && \theta'>90^\circ
\end{aligned}\right\} \tag{2.7}$$

where the first equation is for the growing stage, the second for the decaying stage and the third for the opposite wind. And where S is the two-dimensional energy spectrum, C_g the group velocity of the wave component, A and B the linear and exponential growth rates respectively, θ' the angle between direction of wind and wave propagation, $\Gamma(\theta')$ the angular distribution of two-dimensional spectral density, D the numerical constant which represents the energy dissipation, and S_∞ the fully developed spectrum. As the rates of wave growth A and B the empirical formula of Inoue (1967) are used for expedience. $\Gamma(\theta')$ is replaced by the rule of $\cos^2\theta$. The fully developed spectrum S_∞ is assumed to be given by the function described by PIERSON and MOSKOWITZ (1964): that is;

$$S_\infty(\omega)=\frac{\alpha g^2}{\omega^5}e^{-\beta\left(\frac{g}{U\omega}\right)^4} \tag{2.8}$$

where α and β are the numerical constant, ω the angular frequency, and g the gravitational acceleration.

3. Coastal wave model

It has been confirmed that the comparatively accurate description of the wave situation in the oceans adjacent to coastal regions are obtained by means of the above-mentioned ocean wave model. But a detailed description of the wave conditions in a coastal region is more difficult to obtain for a number of reasons: Japan is surrounded by sea on all sides and the shape of coastal line is complicated; and the total length is approximately 30,000 km.

To compute the wave spectra for all coastal regions would therefore consume a vast amount of computer resources because the computation needs very fine grid size and small time step. Another problem is that we cannot obtain marine surface wind data which is acculate and of sufficient spatial density to justify the computation of such a fine resolution model. In these circumstances, some simplified model is sought for operational coastal wave forecasting.

After some considerations, we developed a model for the coastal waves prediction in which wind waves and swell are computed separately. For the estimation of wind waves and swell we use the characteristic significant wave method and the spectral method respectively.

The grid interval of 10 km was chosen as a compromise between good coastline-shape resolution and computer capability. Only deep water waves are treated as the grid interval of 10 km does not allow for accurate treatment of shallow water waves.

3.1 Computation of swell

(a) The table of dissipating ratio: $c(\mathbf{X}, \theta)$

The wave energy which is generated over the outer ocean and enters the coastal area is transformed and dissipated by islands, peninsula and cape. The dissipation at a selected point depends only on the direction of the intruding propagation energy. So we can define a dissipating ratio $c(\mathbf{X}, \theta)$ as the ratio of the wave energy at a selected point in the coastal region versus the energy incomming through the outer boundary. We calculated and tabulated them previously for routine operation.

We use the second equation of (2.7) for calculation of the dissipating ratio table, i.e.;

$$\frac{\partial S}{\partial t} = -C_g \cdot \nabla S - \mathrm{D} f^4 S \tag{3.1}$$

where $S(\mathbf{X}, t, f, \theta)$ is the two-dimensional energy spectrum defined as a function of position $\mathbf{X}$, time t, frequency f and traveling direction θ. Other variables are the same as before.

Before applying the coastal wave forecast model a coastal area was selected and a 42 by by 32-grid point array (10 km spacing between adjacent points) is arranged over this area.

At first, the wave energy at all sea points is set to zero. Next, constant energy at a given direction is supplied continuously from the outer boundary, and the energy propagation is calculated by integrating equation (3.1).

The adopted energy spectrum has a peak at 10 seconds, based on the assumption that this value is generally representative of the wave period from the outer ocean. The computation is discontinued when the energy levels of all grid points reach saturation. In this way the dissipating ratio is obtained as the value of grid energy divided by the boundary energy.

Using directional energy distribution of $\cos^2\theta$ law, we can remake this ratio to the dissipating rate of wave height. As an example, Fig. 2 shows the contour map of dissipating rate of wave height. In this map dotted areas indicate land.

(b) Swell estimation

Fig. 3 shows a conception of the swell calculation. Arrows marked on the outer boundary express the direction of wave energy which propagates from boundary to the grid point $\mathbf{X}$. $S(\mathbf{X}, \theta, f)$ shows the two dimensional energy spectrum which is defined as a function of position $\mathbf{X}$, traveling direction θ and frequency f. It is assumed that S is given as follows;

$$S(\mathbf{X}, \theta, f) = c(\mathbf{X}, \theta)\ S(\mathbf{X}_0, \theta, f) \tag{3.2}$$

where $c(\mathbf{X}, \theta)$ is the dissipating ratio of energy in direction θ and position $\mathbf{X}$, and $S(\mathbf{X}_0, \theta, f)$ is the spectral component at position $\mathbf{X}_0$ on the outer boundary of calculating area, and which is supplied from the calculation over the outer ocean. Total spectral density $E(\mathbf{X})$ at position $\mathbf{X}$ is expressed as follows;

$$E(\mathbf{X}) = \iint S(\mathbf{X}, \theta, f)\mathrm{d}f\mathrm{d}\theta \tag{3.3}$$

We convert $S(\mathbf{X}, \theta, f)$ to three simplified parameters of swell as follows. Significant wave height is computed from spectral density as follows;

$$H_S = 2.83\ \sqrt{E} \tag{3.4}$$

As a parameter which represents period, we selected the period at which the one dimensional

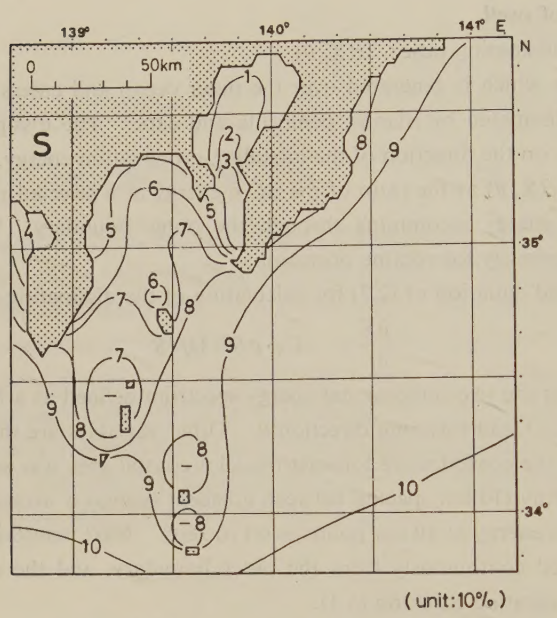

Fig. 2. An example of dissipating rate of wave height. (propagating direction; S)

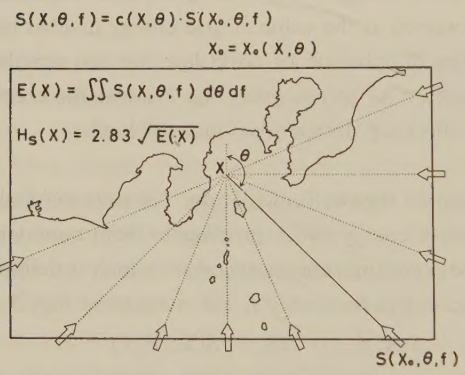

Fig. 3. A concept of the swell calculation.

spectral energy density is maximum. As a wave direction at a point **X**, we choose the direction in which energy is most concentrated. In this way, wave height, period and wave direction of swell over each grid point in a computation area are given.

3.2 Computation of wind waves

(a) Assumption of a marine surface wind

Before computing wind waves in coastal areas, it is necessary to estimate the local marine surface wind blowing over the domain.

1) We use wind data from the meteorological model which is 12 layer, fine mesh (127 km grid interval) limited area model. Initially approximate values of marine surface wind (u', v') at a point are defined as follows;

$$\left.\begin{aligned} u' &= \sum_{k=1}^{m} w_k u_k / \sum w_k \\ v' &= \sum_{k=1}^{m} w_k v_k / \sum w_k \end{aligned}\right\} \tag{3.5}$$

where u_k, v_k (k=1, .., m) are the wind components of fine mesh grid, m the number of grid point and w_k the weighting functions.

2) We use wind data from land station near the shore, and a second set of approximate values of marine surface wind (u'', v'') are defined as follows;

$$\left.\begin{aligned} u'' &= \Big(\sum_{k=1}^{m} w_k u_k + \sum_{l=1}^{n} w_l u_l\Big)/\Big(\sum w_k + \sum w_l\Big) \\ v'' &= \Big(\sum_{k=1}^{m} w_k v_k + \sum_{l=1}^{n} w_l v_l\Big)/\Big(\sum w_k + \sum w_l\Big) \end{aligned}\right\} \tag{3.6}$$

where u_l, v_l (l=1,.., n) are the wind components of each land observation. n the number of stations and w_l the weighting functions. We deal with several points with m and n.

Finally, wind direction at a point is calculated from the values of u'' and v'', and wind speed is calculated by;

$$V=(w_0 V''+w_1 V')/(w_0+w_1) \tag{3.7}$$

where

$$w_0=\sum_{k=1}^{m} w_k + \sum_{l=1}^{n} w_l$$

$$w_1=\min\,(1.0,\ V'')$$

$$V'=\sqrt{u'^2+v'^2}$$

$$V''=\sqrt{u''^2+v''^2}$$

In this way, we estimate marine surface wind at all grid points in the coastal area.

(b) The effective fetch and estimation of wind wave.

Wave generation is limited by the wind fetch which varies largely due to the influence of the coast line configuration such as islands, peninsulas and capes.

So the objective determination of the wind fetch is required for the wave calculation, and we introduce an "effective fetch" F_e shown in Fig. 4. The effective fetch at a point for a wind direction θ is defined as;

$$F_e(\theta)=\sum_i F_i \cos^2\theta_i / \sum \cos\theta_i \tag{3.8}$$

where F_i is the distance between the point and the coast line at an angle of θ_i from the wind direction. The summation on the right hand side of the equation is done over an angle of 45 degrees of both sides of the wind direction. The length of an effective fetch is determined and previously stored in the computer memory for each grid points and wind directions. Fig. 5 shows an example of an effective fetch contour map.

For the calculation of wave generation on each grid points over the coastal area by the

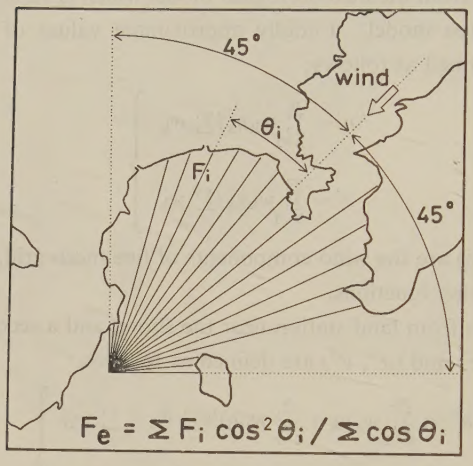

Fig. 4. A concept of an "Effective Fetch" calculation.

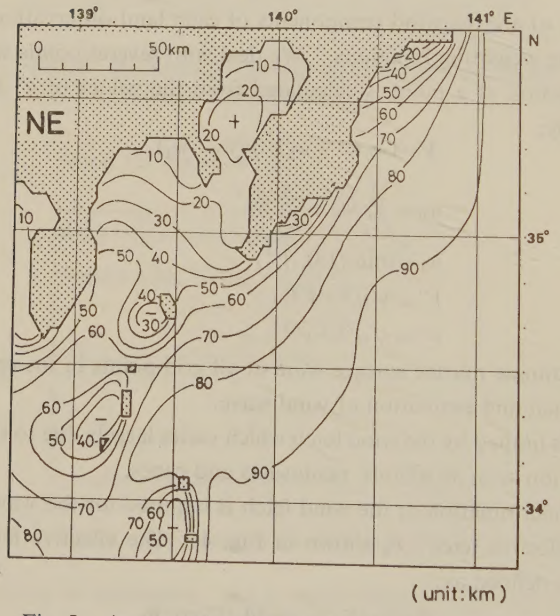

Fig. 5. An example of an effective fetch contour map. (wind direction; NE)

use of above determined wind data and effective fetch, Willson's formula (WILLSON, 1965) is adopted, that is;

$$\frac{gH_w}{V^2}=0.30\left[1-\left\{1+0.004\left(\frac{gF_e}{V^2}\right)^{1/2}\right\}^{-2}\right] \tag{3.9}$$

where H_w is the significant wave height, V the wind speed (m/sec), g the acceleration of

gravity (m/sec^2) and F_e the effective fetch (meter).

The direction of wind wave is that of the marine surface wind, and the period of the wave is computed by the equation of WILLSON (1965) as follows;

$$\frac{gT_w}{2\pi V}=1.37\left[1-\left\{1+0.008\left(\frac{gF_e}{V^2}\right)^{1/3}\right\}^{-5}\right] \tag{3.10}$$

where T_w is the significant period of wind wave. In this way wave height, period and wave direction of wind wave over each grid point are computed.

3.3 Wave estimation for coastal areas

We have described the derivation of swell information in section 3.1 and of wind wave information in section 3.2. Final wave information at a grid point is defined as follows;

(1) Wave height is assumed as combined wave height by using the following equation;

$$H=\sqrt{H_w^2+H_s^2} \tag{3.11}$$

(2) The predominant wave period is given by the period of the higher wave between wind wave and swell, that is

$$T=\begin{cases} T_s & (\text{in case of } H_s \geq H_w) \\ T_w & (\text{in case of } H_s < H_w) \end{cases} \tag{3.12}$$

where T_s is the period of swell and T_w is that of wind wave.

(3) The predominant wave direction is given by the direction of the higher wave between wind wave and swell, that is

$$D=\begin{cases} D_s & (\text{in case of } H_s \geq H_w) \\ D_w & (\text{in case of } H_s < H_w) \end{cases} \tag{3.13}$$

where D_s is the direction of swell and D_w is that of wind wave.

4. Operational implementation of wave forecasts in the JMA

The numerical model in the JMA consists of three steps which are connected from a large grid size to a smaller one. These are, as it were, nesting model. The first step uses a coarse mesh (grid interval is 381 km at 60 degrees north latitude), the second a fine mesh (grid interval is 127 km at 60 degrees north latitude), and the last is the estimation of waves for coastal seas of Japan (the grid interval is 10 km at a representative point in the computation area).

4.1 Operation for coarse mesh

In this step the ocean wave model described in sections 2.1 and 2.2 is used for numerical estimation of sea waves. Pressure and temperature just above sea level supplied by atmospheric model called 12-layer hemispheric spectral model are used to compute the gradient wind.

The energy spectrum of sea waves consist of 22 frequency components from 0.04 Hz to 0.25 Hz with 0.01 Hz-interval and of 16 direction components in step of 22.5 degrees. The area of computation are the western North Pacific, Japan Sea, East China Sea and a part of South China Sea shown as A in Fig. 6. The grid size for computation consists of 36 by

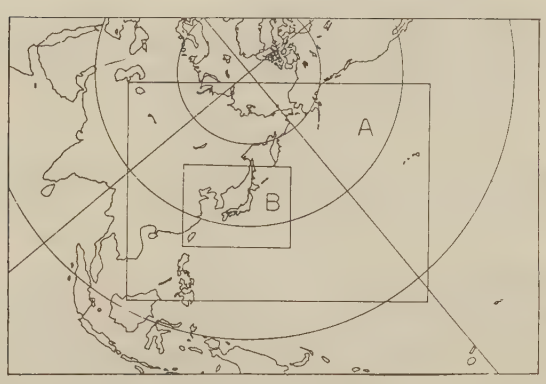

Fig. 6. Calculation area of coarse mesh (region; A) and fine mesh (region; B)

27 grid points and computations are made only at grid points located over the sea. When a grid point is covered by sea ice, the grid point is considered as a land point. The time step interval for calculation is 6 hours and two versions are run. The first is a 24 hour hindcast version and the wave energy spectrum of the last step is used as the initial condition of the forecast version and stored as an initial condition for the next day's hindcast computation. In this version, sea level pressure and air temperature are supplied from the objective analysis and prediction by the atmospheric model. The next is 36 hours forecast version in which the initial condition is prepared by the first version and the meteorological conditions are from the prediction by the atmospheric model.

The energy spectra include various information on the wave condition and are very useful in the precise description of the sea state. But a large number of information are not always convenient to describe the general features of the sea state. So, the results of the model computations are summarized into simplified parameters such as wave height, period and wave direction using the same methods described in section 3.1(b).

Significant wave height is computed from spectral densities as follows;

$$H_{1/3}=2.83\sqrt{E} \tag{4.1}$$

where $$E=\iint S(\theta, f)\mathrm{d}f\mathrm{d}\theta$$

The prevailing period is defined as the period of the one-dimensional spectral peak and the wave direction as the direction in which most energy is concentrated.

Fig. 7 shows flow of operational numerical wave model in the JMA. The ocean wave information produced using the procedure are broadcast by radio facsimile as the wave analysis chart and the wave forecast chart (24 hours prognostic chart) over the western North Pacific. Examples of the products are shown in Fig. 8 and Fig. 9.

Fig. 8 is the wave analysis chart at 00Z, Sep. 24, 1983 made by the model calculation and ship observations. Fig. 9 is the 24 hr-forecasting chart made at 00Z, Sep. 23, 1983. Comparison of both figures shows reasonable agreement between prediction and observation.

Because of the relatively long time step and coarse resolution of the atmospheric model,

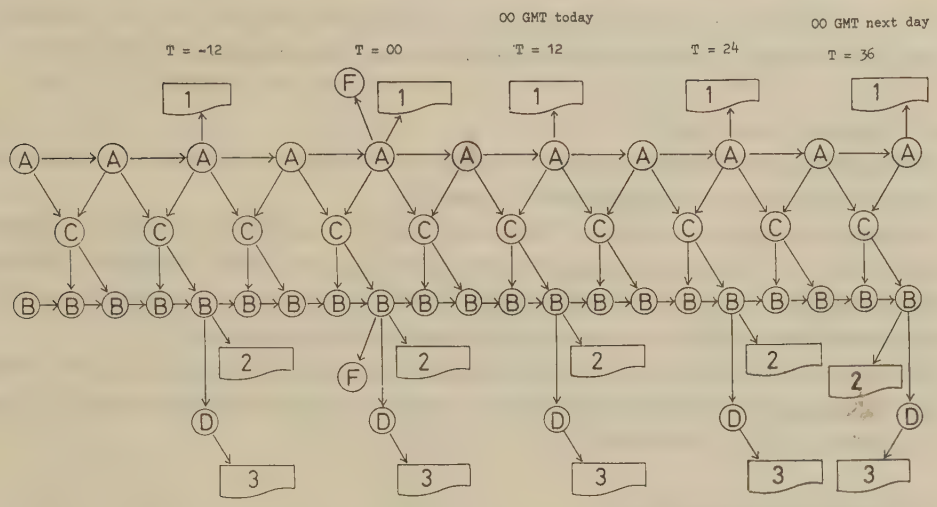

Fig. 7. Calculation flow of wave model in the JMA.

A; Calculation of coarse mesh model over the western North Pacific
B; Calculation of fine mesh model over the adjacent sea of Japan
C; Interpolation
D; Calculation of coastal model around Japan
F; Data for next day's calculation
1; Print-Out of products of the western North Pacific
2; Print-Out of products of the adjacent sea of Japan
3; Print-Out of products of the coastal sea of Japan
where 1, 2, 3 & D are made every 6 hours

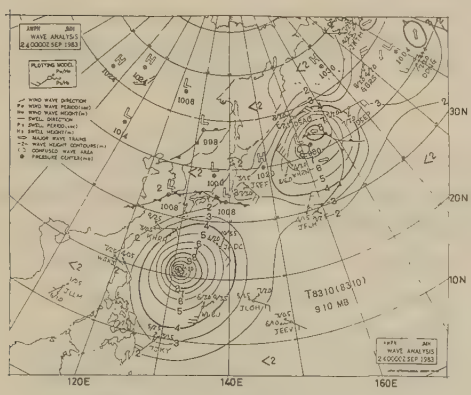

Fig. 8

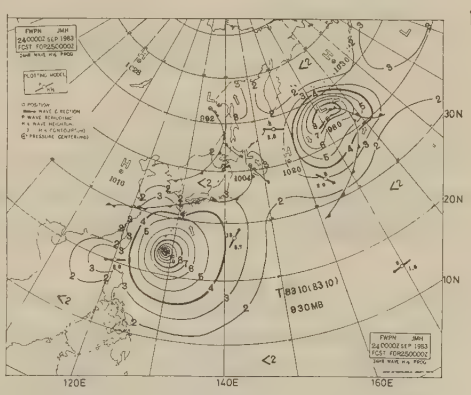

Fig. 9

Fig. 8. Wave analysis chart over the western North Pacific.
Fig. 9. Wave forecast chart over the western North Pacific.

the ocean wave model is not capable of predicting very high waves generated in typhoons and rapidly developing lows. Manual corrections are made empirically based on the sea situation, ship observations and the forecast chart of surface pressure.

If a typhoon structure is predicted by means of Fujita's formula (FUJITA, 1962), objective correction of waves in typhoon area can be made in our ocean wave model (UJI, 1975).

4.2 Operation for fine mesh

The method which estimates the sea conditions for the fine mesh is based on the spectral method similar to that of the coarse mesh procedure.

A calculation area is divided into 37 by 31 grid points, the area of computation is shown as B in Fig. 6. The time step interval is 3 hours and the sea level pressure and the air temperature just above sea level are prepared from the atmospheric model (12-layer fine mesh limited area model) as the basic external data for wind calculations.

Computational conditions on the outer boundary are provided by the spatial and temporal interpolation of the products from the coarse mesh model taking one half the time step and one third the grid interval.

4.3 Operation for coastal waves

Fig. 10 shows the general flow chart of the operational coastal wave model mentioned in section 3. The table of the dissipating ratio for wave energy and the table of the effective fetch are stored on a disk and are refered to as they are needed. In the estimation of the sea surface winds in coastal areas, winds of land stations are used only in the hindcast version and winds from the atmospheric model are used at any time. Calculations are carried out

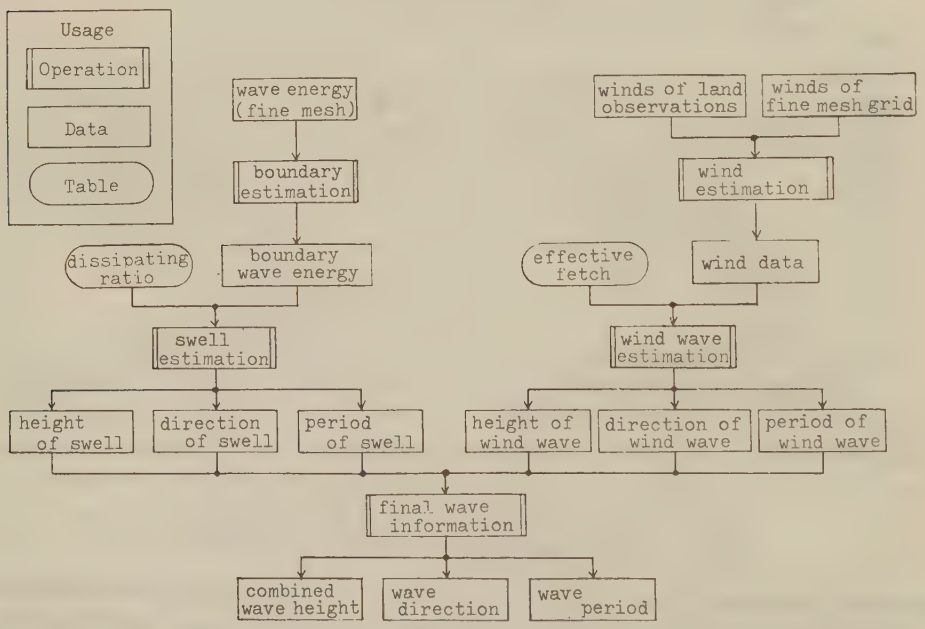

Fig. 10. General flow chart of the coastal wave model.

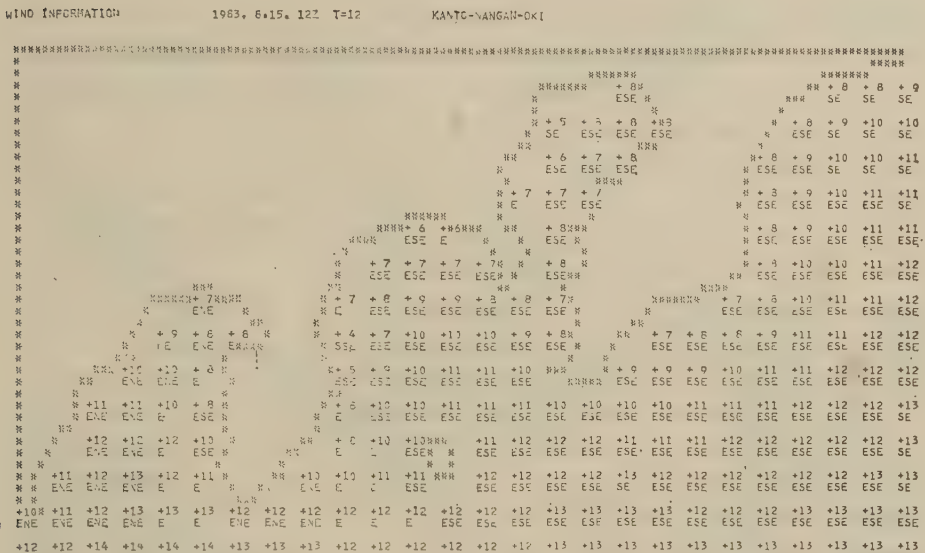

Fig. 11. An example of sea surface wind informations of coastal area. '+' mark shows a grid point (interval of each grid is 10 km), group of numerals (upper) and alphabets (lower) wind speed and direction respectively.

for about 12 coastal areas around Japan which include imptorant ports and harbors. Each coastal area is divided into 42 by 32 grid points with the grid interval of 10 km. As shown in Fig. 7, the coastal wave model forecast system output some list every 6 hours interval and the following are produced for coastal areas:

1) Sea surface wind (direction and speed) information. Examples are shown in Fig. 11.
2) Wave information (significant wave height, prevailing wave period and direction) which are shown in Fig. 12 as example.
3) Time sequence for every 6 hours of wave and wind data at about 120 points.
4) Machine drawn chart of significant wave height for all coastal areas.

Fig. 13 shows an example of the analysis chart of the coastal sea area prepared routinely by the JMA for broadcast. Configuration of the forecast chart of the coastal sea areas is the same as the analysis chart except for the data of coastal wave-recorders. These charts are transmitted to local meteorological offices by land-line telecommunication system (not by radio facsimile) once a day.

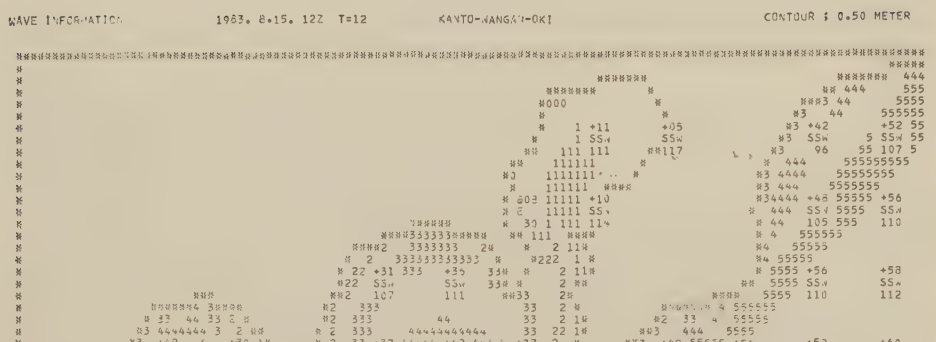

Fig. 12. An example of wave informations of a coastal area. Group of alphabets and numerals show significant wave height (upper), wave direction (middle) and wave period (lower). Grid interval of this map is 20 km and group of same numbers shows contour line of wave height.

When forecasters of a local meteorological office formulates forecasts and warnings for weather and waves in the coastal areas, these staff would then refer to the wave analysis and forecast charts to increase the accuracy of their results.

5. Evaluation

5.1 Wind and wave caused by Typhoon

Among severe meteorological situations, typhoon is considered as one of the most severe meteorological phenomena affecting the safety and economy of ships. Thus it is very important to make an acculate prediction of the distribution of wave conditions in a typhoon area. As an example we compared our model estimation with the observations which was made when Typhoon 8013 Orchid passed through west of Japan from south to north on 11, Sept. 1980. Fig. 14 shows the track of Typoon 8013 Orchid.

Fig. 15 shows the time variation of wind speed and significant wave height of the ocean data buoy (25.67N, 135.92E) and hindcast data of our fine mesh wave model respectively.

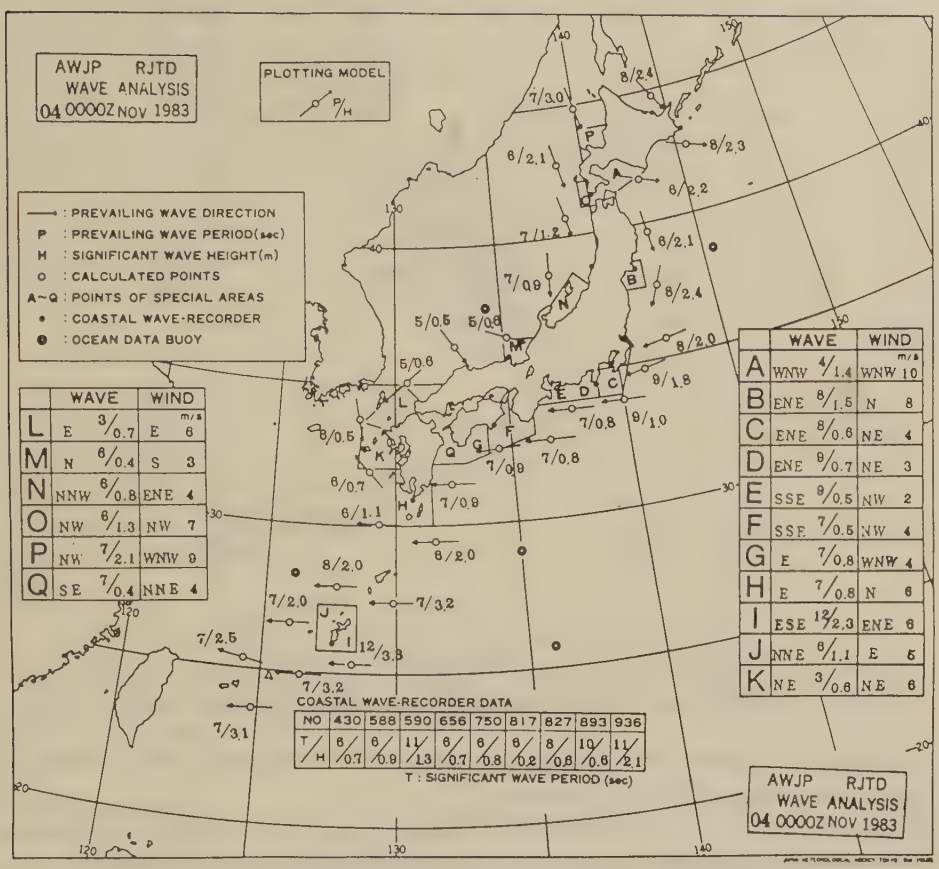
AWJP RJTD
WAVE ANALYSIS
04 0000Z NOV 1983
PLOTTING MODEL
P/H
: PREVAILING WAVE DIRECTION
P : PREVAILING WAVE PERIOD(sec)
H : SIGNIFICANT WAVE HEIGHT(m)
o : CALCULATED POINTS
A~Q : POINTS OF SPECIAL AREAS
• : COASTAL WAVE-RECORDER
● : OCEAN DATA BUOY
WAVE WIND
L E 3/0.7 E 6
M N 6/0.4 S 3
N NNW 6/0.8 ENE 4
O NW 6/1.3 NW 7
P NW 7/2.1 WNW 9
Q SE 7/0.4 NNE 4
WAVE WIND
A WNW 4/1.4 WNW 10
B ENE 8/1.5 N 8
C ENE 8/0.6 NE 4
D ENE 9/0.7 NE 3
E SSE 9/0.5 NW 2
F SSE 7/0.5 NW 4
G E 7/0.8 WNW 4
H E 7/0.8 N 6
I ESE 12/2.3 ENE 6
J NNE 6/1.1 E 5
K NE 3/0.6 NE 6
COASTAL WAVE-RECORDER DATA
NO 430 588 590 656 750 817 827 893 936
T/H 6/0.7 6/0.9 11/1.3 6/0.7 6/0.8 6/0.2 8/0.8 10/0.6 11/2.1
T : SIGNIFICANT WAVE PERIOD (sec)
AWJP RJTD
WAVE ANALYSIS
04 0000Z NOV 1983

Fig. 13. Analysis chart of the coastal sea area.

In the process of computation of fine mesh wave model the typhoon correction model was applied.

Variation of wind speed by the model estimation agrees well with the buoy observations. The prediction of wave height also agrees reasonably well with the observations, however it has systematic descrepancies, that is slower growth and decay than the observations and lower estimation of wave height during the most severe wave conditions. The descrepancies may be due to the smoothing effect of finite time step and grid interval which are used in the prediction equation. The 127 km-grid interval and 3 hours-time step are not sufficient to represent the complicated meteorological and maritime conditions near a typhoon center.

Fig. 16 shows the time variation of wind of an observation point and a grid near the point by coastal wave model throughout the typhoon passage. The observation point is Shionomisaki Observatory (see Fig. 14) which is located at the southern tip of Kii-Peninsula. Based on our experience wind speed estimated by our fine mesh model has a higher value

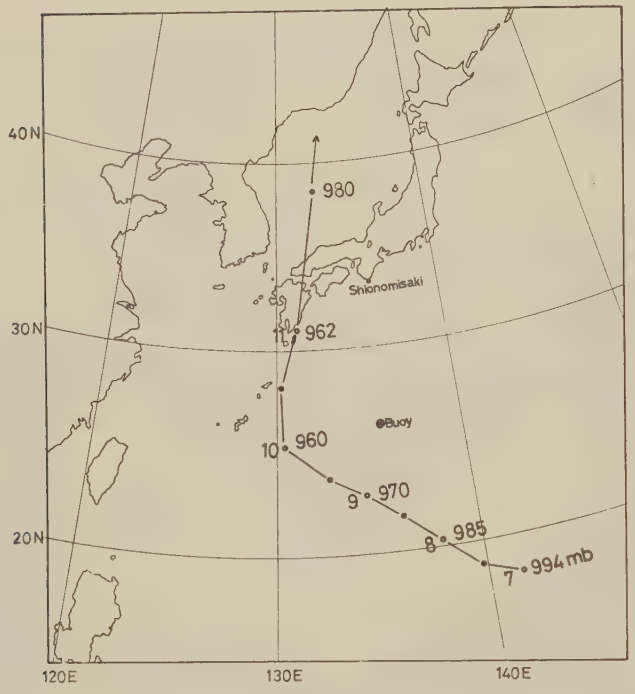

Fig. 14. Track of the Typhoon 8013 Orchid from 7 to 11 Sep. 1980.

than that actually observed near the coast, because our fine mesh model does not incorporate topographical effects in the wind estimation.

The winds used in the coastal wave prediction are estimated by the spatial interpolation method with the wind of the fine mesh model and land observations by eq. (3.7).

Overestimated wind speed values during the typhoon passage are shown in Fig. 16 (lower). Before and after this period estimated wind speeds agree fairly well with the observations. As shown in the upper part of Fig. 16 almost all estimations of the wind direction generally coincide with observations. The accuracy of the wind direction is very vital in the determination of the effective fetch which is one of the major parameters of the coastal wave estimation.

5.2 Comparison with coastal wave observation

The JMA has spread the network of coastal wave-recorders since 1977 and is now routinely operating 10 stations as shown in Fig. 17. The coastal wave-recorders are the ultrasonic type and set at a depth of about 50 meters off the respective coast. The records are taken at 0.5 second-interval over 20 minutes every three hours, and statistics of wave height and wave period are calculated routinely.

We evaluated the coastal wave model by comparing the estimated values of the significant wave height with the observation from the above mentioned coastal wave recorders. The

Fig. 15. Time valuation of wind speed (upper) and significant wave height (lower). Full line; the ocean data buoy (25.67N, 135.92E) and dotted line; hindcast data of the model. Period; 6 to 13 Sep. 1980.

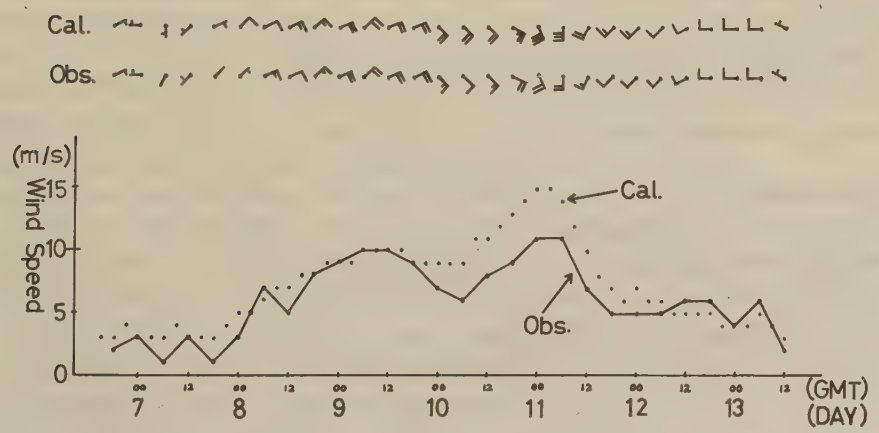

Fig. 16. Valuation of winds at the Shionomisaki Observatory (Wakayama Prefecture and the hindcast data of the model. Upper shows wind direction and lower wind speed. Period; 7 to 13 Sep. 1980.

comparison was made after a year routine operation from March 1983 to February 1984, and the results are shown in Table 1.

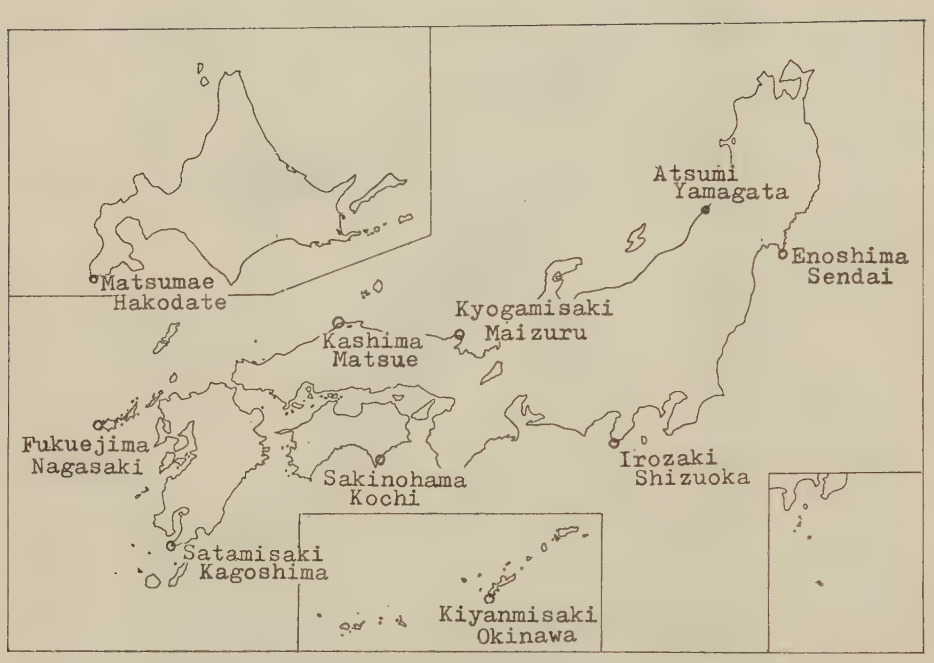

Fig. 17. Network of coastal wave-recorder in the JMA.

Table 1. Comparison of significant wave height between coastal wave-recorder and model output from Mar. in 1983 to Feb. in 1984.

STATION	T = 12							T = 36						
	n	Mean		σ		γ	RMS	n	Mean		σ		γ	RMS
		Obs.	Cal.	Obs.	Cal.				Obs.	Cal.	Obs.	Cal.		
Matsumae	355	0.97	1.21	0.76	0.79	0.84	0.42	354	0.97	1.53	0.76	0.98	0.82	0.43
Atsumi	358	1.19	1.23	1.09	0.91	0.89	0.49	357	1.19	1.48	1.10	1.09	0.86	0.55
Kyogamisaki	359	1.12	1.29	0.95	0.93	0.91	0.39	358	1.12	1.50	0.95	1.08	0.87	0.47
Fukuejima	359	1.15	1.31	0.83	0.87	0.84	0.45	358	1.15	1.40	0.83	0.95	0.75	0.55
Enoshima	363	1.32	1.42	0.78	0.66	0.75	0.51	362	1.32	1.43	0.78	0.77	0.71	0.54
Irozaki	356	1.27	1.32	0.76	0.85	0.72	0.53	355	1.27	1.44	0.76	0.89	0.74	0.51
Sakinohama	352	0.91	1.06	0.61	0.82	0.69	0.44	351	0.91	1.08	0.61	0.90	0.69	0.44
Satamisaki	353	0.79	1.11	0.48	0.64	0.71	0.34	352	0.79	1.22	0.48	0.69	0.64	0.37
Kiyanmisaki	319	0.95	1.65	0.53	1.03	0.69	0.39	318	0.95	1.64	0.53	0.87	0.69	0.39

where (n) is data amount, (σ) standard deviation, (γ) correlation coefficient, RMS root mean square error, Obs. observation value of a coastal wave-recorder, Cal. model output.

In this table, the upper four stations are located on the coast of the Japan Sea and the lower five stations are on the Pacific coast (see Fig. 17). T=12 and T=36 represent the results of 12 hours predictions and 36 hours predictions respectively.

Observed annual means of the significant wave height are lower than that of the model prediction, but the discrepancy is not so large.

In our coastal wave model, wind waves over the coastal area are assumed to be saturated with respect to the wind direction, and the wave heights are determined by the effective fetch and wind speed because of the narrowness of the coastal area. This may at times result in the overestimation of the wave height.

As for the correlation coecffiient in Table 1, the predictions have rather higher correlation to the observations at the stations on the Japan Sea coast than on the Pacific coast. The reason is that the Japan Sea is a closed basin and the effect of swell on the coastal waves can be well defined but in the Pacific the swell effect can only be roughly estimated because of its wideness. Seasonal characteristics of the present evaluations, which are not shown in Table 1 however, are that the correlations at the Japan Sea coast are higher in the cold season due to the prevailing northwest winter monsoon than during the warm season. On the other hand, the reverse is the case at the Pacific coast during the southerly summer wind season.

6. Concluding remarks

The numerical wave prediction model which has been used in the JMA since 1983 consists of a coarse mesh model, a fine mesh model and a coastal wave model. The coarse mesh model and the fine mesh model are almost the same as the ocean wave model which has been used routinely for the western North Pacific in the JMA since 1977. In the coastal wave model, wind waves and swell are calculated separately and computed thereafter. These models are used successfully through the last two years, but some revision are planned as follows,

1) Extension of wave forecasting period in the ocean.
   24 hour predictions are made at present, but 4 days or one week predictions are desired in the field of ship routing and coastal engineering.
2) Extension of wave analysis and forecast areas in the coastal wave prediction.
   At present the results of analysis and forecast are presented on the representative point in each of 12 selected sea area. It is now deemed necessary that the wave distribution be presented over the selected coastal areas, and the selected area should be extended to cover all of the Japanese coast.
3) Introduction of new ocean wave model.
   In our ocean wave model which is used since 1977, a linear spectral wave model is adopted. Based on the recent theoretical and experimental studies of wind wave generation, the linear spectral model will be replaced by a coupled discrete mode which was developed at the MRI (Uji, 1983).
4) Improvement of wind analysis method.

Wind estimation at present depends on the pressure and temperature of the atmospheric model. By incorporating ship observations, we hope to have better forecast accuracy in the wind estimation.

Acknowledgements

The authors wish to express their hearty thanks to Dr. I. Isozaki of the Meteorological Research Institute for his encouragement and careful reading of this manuscript.

The coastal wave model was completed as a joint effort of Messrs. H. Onoda, K. Tonomura, K. Sakurai, T. Kikuchi and the MRI staff through the last five years.

References

Blackadar, A. K. (1965): A simplified two-layer model of the baroclinic neutral atmospheric boundary layer. Air Force Cambridge Res. Lab. Report, **65-531**, 49–65.

Cardone, V. J. (1969): Specification of the wind distribution in the marine boundary layer for wave forecasting. New York Univ. School of Engineering and Science, Report GSL-TR-**69-1**, 131

Fujita, T. (1962): Pressure distribution within typhoon. Geo. Mag. **23**, 437–451.

Inoue, T. (1967): On the growth of the spectrum of a wind generated sea according to a modified Miles-Phillips mechanism and its application to wave forecasting. Geophy. Sci. Lab. Report TR-**67-5**, New York Univ., 74.

Isozaki, I. and Uji, T. (1973): Numerical prediction of ocean wind waves. Papers in Met. and Geophys., **24**(2), 207–231.

Isozaki, I. and Uji, T. (1974): Numerical model of marine surface winds and its application to the prediction of ocean wind waves. Papers in Met. and Geophys., **25**(3), 197–231.

Pierson, W. J. and L. I. Moskowitz (1964): A proposed spectral form for fully developed sea based on the similarity theory of S. A. Kitaigorodskii. J. Geophy. Res., **69**, 5181–5190.

Uji, T. (1975): Numerical estimation of the sea wave in a typhoon area. Papers in Met. and Geophys., **26**(4), 199–217.

Uji, T. (1983): The sea wave prediction model MRI-II. Dr. Thesis, Tohoku Univ.

Willson, B. W. (1965): Numerical prediction of ocean waves in the Morth Atlantic for Dec. 1959. Deut. Hydrogr. Z., 18.

気象庁が開発した沿岸波浪数値予報モデルについて

竹内昌明・高田政幸

（気象庁　海上気象課）

気象庁海上気象課は NWW 計画の一環として，1979年沿岸波浪数値予報モデルの開発に着手し，気象研究所海洋研究部の多大な協力を得て 1982 年完成した．その後，実用試験・業務実験を経て 1983年 3 月沿岸波浪予報の運用が開始された．この結果，外洋（北西太平洋を対象とし，格子点間隔 381 km），近海（日本近海を対象とし，格子点間隔 127 km）および沿岸（特定の海域を対象とし，格子点間隔 10 km）のそれぞれの波浪モデルを連結して計算することにより，外洋から沿岸に至る一連の波浪予報システムが確立された．沿岸波浪数値予報モデルの特徴は，外洋波浪数値予報モデルにおける波エネルギーの時間積分による波浪推算法と異なり，うねりの算出にはスペクトル法を，風波については有義波法を用いて診断的に波浪推算を行う点にあり，この手法を採用することにより，計算機負荷の軽減をはかり，沿岸波浪予報のルーチン化を可能にした．ある特定の海域における計算領域は 420×320 km （陸地を含む）であり，これら海域が現在主要港湾を含む12か所に設定されていて，日本の沿岸の約 50% に相当する範囲について計算を行っている．本稿では，波浪予報システムの概要および検証結果について報告する．

The Oceanographical Magazine
Vol. 35, Nos, 1-2, pp. 21 to 29, March 1985

Frontal eddies observed in the East China Sea in May and October of 1982

Akira SHIBATA
Meteorological Research Institute
and
Ippei EGUCHI
Nagasaki Marine Observatory

(Received September 20, 1984; Accepted January 10, 1985)

Abstract: In 1982 oceanographical observations around the shelf edge in the East China Sea were carried out by a research vessel of the Nagasaki Marine Observatory. By two surveys conducted in May, existence of the cyclonic eddies as observed from the IR satellite images was confirmed. The eddies have folded wave patterns, and this folding structure as observed in the surveys appears to be related with effective mixing of the shelf and Kuroshio waters. Inside of the eddy both the shelf and Kuroshio waters seem to ascend with cyclonic rotation. Eddies were also found in the surveys in October. It is difficult, however, to describe their detailed structure because of possibly smaller scale of the eddies than those in May.

1. Introduction

Recently eddies are observed from the IR satellite images around the shelf edge in the East China Sea always in winter and spring (AKIYAMA et al. (1982), SHIBATA (1983)). According to the IR satellite images a horizontal size of the eddy is estimated at about 30 miles across and about 100 miles along the Kuroshio stream. It is natural that such eddies have not been caught by JMA's routine observations along one observational line (PN line, see Fig. 1), since intervals of the stations are usually 10–30 miles. So far, two special surveys around the shelf edge have been made by JMA: one was made in autumn of 1968 by five research vessels, and the other was made in autumn of 1974 by one research vessel (SAWARA and HANZAWA (1979)). Unfortunely the eddies were not caught definitely either by those observations, because the difference in temperature between the shelf and Kuroshio waters is relatively small in this season of the year. No observations have ever been made in spring when the difference in temperature is relatively large. Although existence of such eddies have not been confirmed by research vessels, eddies were already conjectured on the ground of large horizontal shear across the Kuroshio boundary (TSUJITA and KONDO (1957)). But as we will see later, besides the shear, the bottom effect may be another cause of the eddies.

It is observed from the IR satellite images that the eddies have folded wave patterns (SHIBATA, 1983). This folding structure appears to be related with effective mixing of the shelf and Kuroshio waters. By means of the T-S diagrams, SAWARA and HANZAWA (1979)

discussed mixing processes, using data obtained in the special surveys in 1968 and 1974. One of their results is that an area where mixing is likely to occur exists along the shelf edge at the depth of about 100 m. They supposed that the bottom water on the shelf may intrude into the Kuroshio around the shelf edge at the depth of about 100 meters and mixing after intrusion may take complicated processes. At the present stage the relationship between the eddies and mixing processes is not well understood.

The eddies observed in the IR satellite images in the East China Sea appear to be similar to the frontal eddies in the western boundary of the Gulf Stream between Miami and Cape Hatteras (Lee et al. (1981)). Features of the frontal eddy in the Gulf Stream are summarized as follows: horizontal size; 20 miles across and 50–100 miles along the Gulf Stream, lifetime; 2–3 weeks, and traveling speed to the north; 0.4 m/s. The frontal eddies form from unstable wave-like meanders of the Gulf Stream cyclonic front. But the exact nature of the instability is uncertain, because both barotropic and baroclinic unstable waves can develop in the Gulf Stream cyclonic front (Lee et al. (1981)). The horizontal size of the eddy in the East China Sea is estimated from the IR satellite images at about 30 miles across and about 100 miles along the Kuroshio stream. The lifetime of the eddy have not been really estimated from the IR satellite images.

In the East China Sea JMA's buoy has been located around the Kuroshio boundary since September, 1974 (see Fig. 1). Three sensors for water temperature are mounted on the mooring cable of the buoy, and the depth of each sensor is 2, 20, and 50 meters under the surface, respectively. The water temperature observed on the buoy shows a fluctuation with the period of about 10–20 days in winter and spring (Shibata (1983)). The water temperature fluctuates between 16 and 22°C which correspond approximately to the temperature of the shelf and Kuroshio waters, respectively. Therefore 10–20 days are considered to be the period with which a new eddy comes (or appears) after an old eddy leaves (or disappears). No observations of the traveling speed have ever been made from the IR satellite images.

In 1982, the Nagasaki Marine Observatory made a plan to investigate the eddies mentioned above, and surveys were carried out in May and October, 1982. This paper reports the results. The main purpose of the surveys is to confirm the eddy as observed from IR satellite images and describe its structure. For understanding the generation mechanism or the development of the eddy we should wait for more detailed surveys made by multi-research vessels.

2. Observations

Two consecutive observations were carried out in each month of May and October, 1982. The first survey in May was made between the 1st and the 4th, and the second was made between the 15th and the 17th. The survey area covers the shelf edge between lat. 28°N and lat. 30°30′N. It required about 65 hours to complete each survey. Observational stations are marked by solid circles shown in Fig. 2 for the first survey and in Fig. 4 for the second survey. Intervals of the stations were determined with reference to the horizontal size of

the eddy observed from the IR satellite images, as 5–10 miles across and 20 miles along the Kuroshio stream. Temperature profiles were obtained with XBT or Tsurumi Micon-BT. In addition to temperature profiles, salinity profiles were obtained with Tsurumi STD on the X line of the second survey as shown in Fig. 4.

The first survey in October was made between the 10th and the 11th, and the second was made between the 17th and the 19th. The survey area covers the shelf edge between lat. 29°N and lat. 31°N. It required about 45 hours to complete each survey. Observational stations are marked by solid circles shown in Fig. 9 for the first survey and in Fig. 10 for the second survey. Intervals of the stations were the same as those in May. Temperature profiles were obtained with XBT or Tsurumi Micon-BT.

Fig. 1 shows bottom topography, whose data were obtained with observations by the Hydrographic Department of the Maritime Safety Agency and the Nagasaki Marine Observatory. Contour lines are drawn at intervals of 200 meters, but lines for depth deeper than 1200 meters are omitted. A double circle shown in Fig. 1 is indicative of location of the meteorological buoy which JMA has maintained in the East China Sea since September, 1974. An oblique line shown in Fig. 1 is a routine observational line conducted by the Nagasaki Marine Observatory since 1955 (PN line or G line). The Kuroshio flows along the

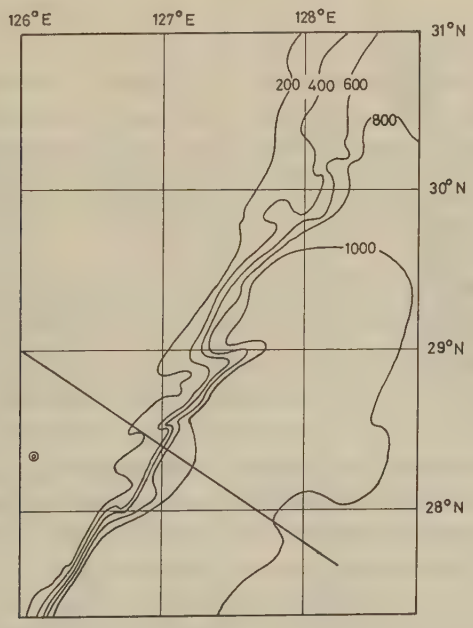

Fig. 1. Bottom topography in the East China Sea. Contour lines are drawn at intervals of 200 meters, but lines for depth deeper than 1200 meters are omitted. A double circle is indicative of location of JMA's buoy, and an oblique line is a routine observational line conducted by the Nagasaki Marine Observatory (PN line or G line).

shelf edge, and turns to the east above about lat. 30°N. According to the routine observations the boundary between the Kuroshio and shelf waters fluctuates along this observational line, whose amplitude is up to 30 miles. This means that the Kuroshio does not flow straightforwardly. It is noticed in the bottom topography that undulations of 400–1000 m. contours exist along the shelf edge. In particular following two bumps may disturb the Kuroshio, since the Kuroshio current reaches to 1000 meters. One bump is around lat. 28°N and long. 126° 40′E, and the other is around lat. 29°N and long. 127°30′N.

3. Results

3.1 Surveys in May, 1982

In the survey areas mentioned above, the difference in temperature between the shelf and Kuroshio waters reaches normally a maximum in March, and later on decreases from southern areas. Even in May the difference in temperature is large enough to distinguish two waters.

Figs. 2 and 3 show water temperature observed in the first survey, whose depth is 0 and

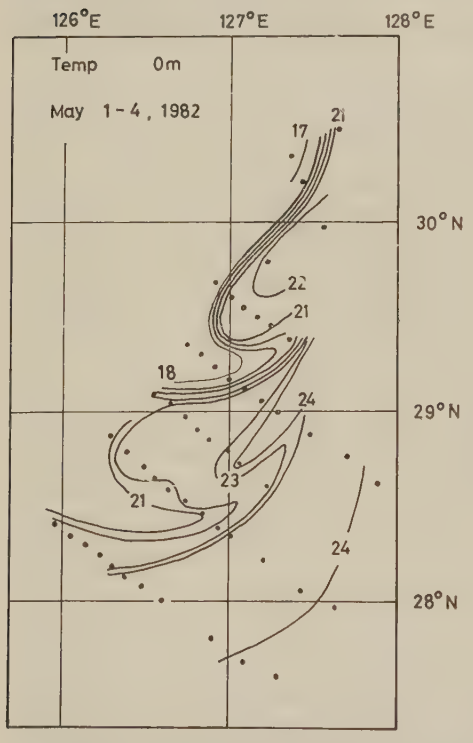

Fig. 2

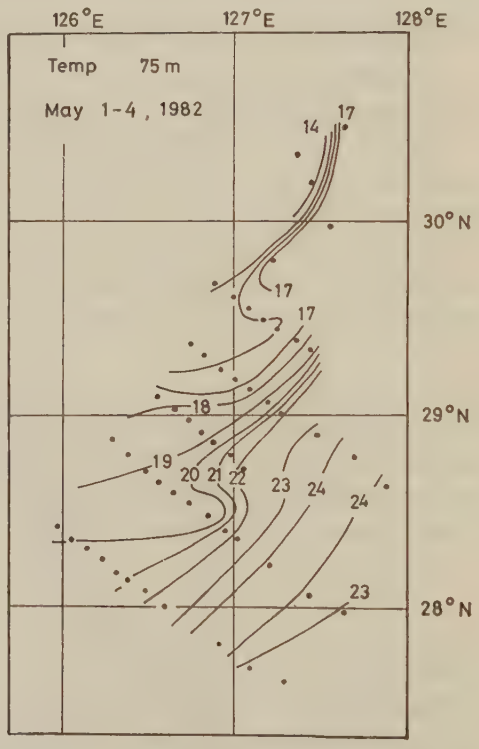

Fig. 3

Fig. 2. Water temperature observed in the first survey in May. Depth is 0 meter. The eddies are found, and a meander of the Kuroshio is noticed.

Fig. 3. Water temperature observed in the first survey in May. Depth is 75 meters.

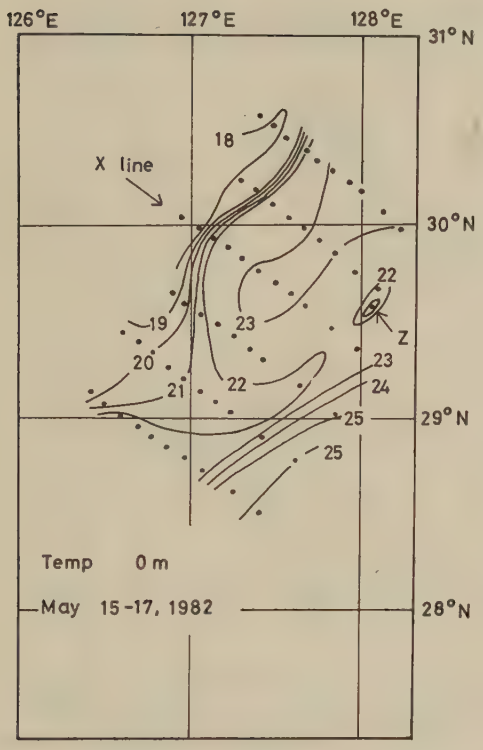

Fig. 4

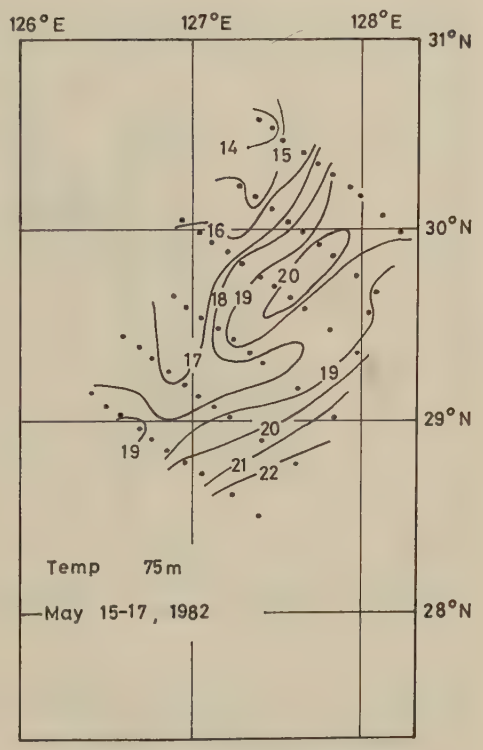

Fig. 5

Fig. 4. Water temperature observed in the second survey in May. Depth is 0 meter. Salinity profiles are obtained on the X line. A station marked by Z is noticed, whose temperature is 20.9°C. The meander of the Kuroshio takes different paths.

Fig. 5. Water temperature observed in the second survey in May. Depth is 75 meters.

75 meters, respectively. Folded wave patterns are found in these figures, and two eddies are noticed. Since these eddies resemble the frontal eddies in the Gulf Stream, we call the frontal eddy also for the eddy in the East China Sea. Comparison of the figures indicates that inside of both eddies the waters rotate cyclonically. It is also noticed that the Kuroshio flows offshore across the PN line (compare Fig. 2 with Fig. 1).

Figs. 4, 5, 6 and 7 show water temperature observed in the second survey, whose depth is 0, 75, 150 and 250 meters, respectively. From these figures it is shown that the Kuroshio flows onshore across the PN line. Therefore a meander of the Kuroshio takes different paths in short intervals of about ten days. A large frontal eddy is noticed. The development of the eddy was not traced, since an interval of about ten days between two consecutive surveys was too large for the lifetime of the eddy and we could not get the IR satellite images in that period. Inside of this eddy the waters rotate cyclonically as observed in the first survey.

The station marked by Z in Fig. 4 is of interest, because the temperature of 20.9°C and

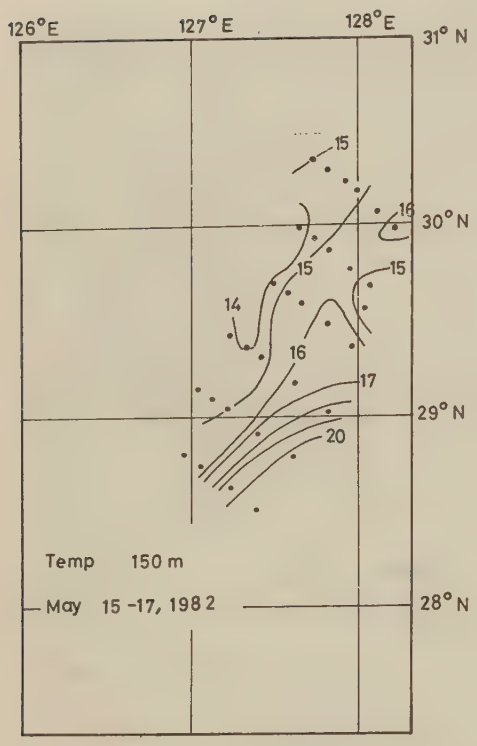

Fig. 6

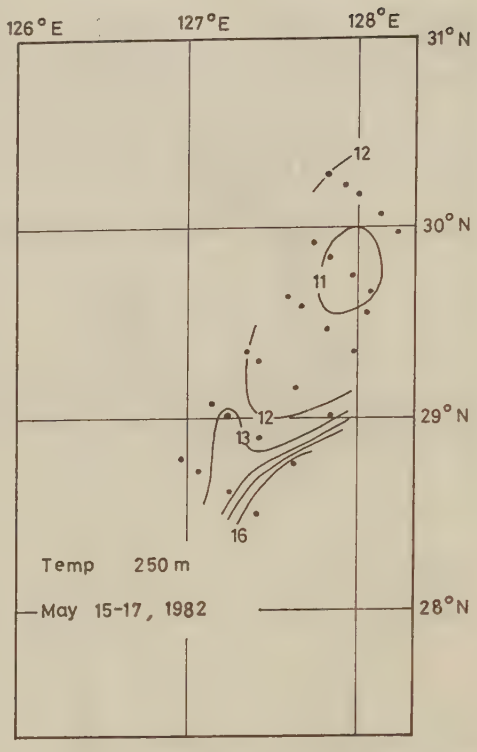

Fig. 7

Fig. 6. Water temperature observed in the second survey in May. Depth is 150 meters.
Fig. 7. Water temperature observed in the second survey in May. Depth is 250 meters.

the salinity of 34.095‰ were observed at the surface of this station. Such isolated water mass of low temperature and low salinity may originate in the shelf waters, since the salinity of the Kuroshio does not fall less than 34.3‰ even at the depth of 1000 meters. Since such low water temperature is not found at the surface upstream from the station Z, this water mass may rise up to the surface from the bottom on the shelf. The same water mass can be caught on the X line located upstream (see Fig. 4). Fig 8 shows a cross-section of salinity on the X line. It reveals that the shelf waters intrude into the Kuroshio at the depth of 50–90 meters as shown at the station of X-b. Therefore the bottom waters on the shelf may intrude into the Kuroshio around the shelf edge. This idea coincides with SAWARA and HANZAWA (1979). Two waters observed on the X line (X-b) and the station Z seem to be directly connected. As shown in Figs. 6 and 7, an area of low temperature exists at the depth of 150–250 meters under around the station Z. If such area of low temperature would indicate upwelling, it might be said that inside the eddy both the shelf and Kuroshio waters ascend with cyclonic rotation.

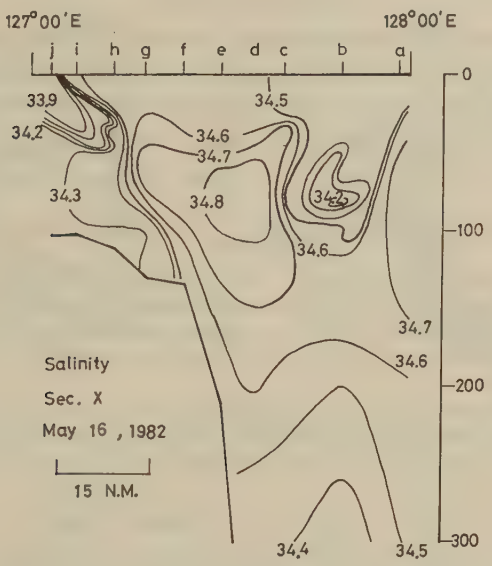

Fig. 8. Salinity observed on the X line in the second survey.

3.2 Surveys in October, 1982

Since the difference in temperature between the shelf and kuroshio waters in autumn is generally smaller than 2–3°C at the surface, these two waters can not be distinguished very well in this season. Moreover a thermocline with vertical temperature difference of about 7–8°C is normally observed at the depth of about 50 meters by the routine observations made by research vessels. Therefore it is difficult to find the eddies in the horizontal map at the depth shallower than about 50 meters.

Fig. 9 and 10 show water temperature at the depth of 75 meters observed in the first and the second survey, respectively. Although features of these patterns are not so clear as compared with those in May, the main feature shown in Fig. 9 is that a zone of low temperature sandwiched between the Kuroshio and shelf waters exists along the shelf edge. This structure was observed also in two special surveys in autumn of 1968 and 1974 (JMA, 1968 and 1974). This structure seems to be normally observed in autumn. In Fig. 10 eddies are found, but their scales are smaller than those in May and their position is shifted onshore.

In the first survey the Kuroshio flows offshore across the line around lat. 30°N, but in the second survey it flows onshore around the same area. Therefore the meander of the Kuroshio takes different paths in short intervals of about seven days.

4 Summaries of the results and discussions

By surveys conducted in May, existence of the cyclonic eddies as observed from the IR satellite images is confirmed. Inside of the eddy both the shelf and Kuroshio waters seem

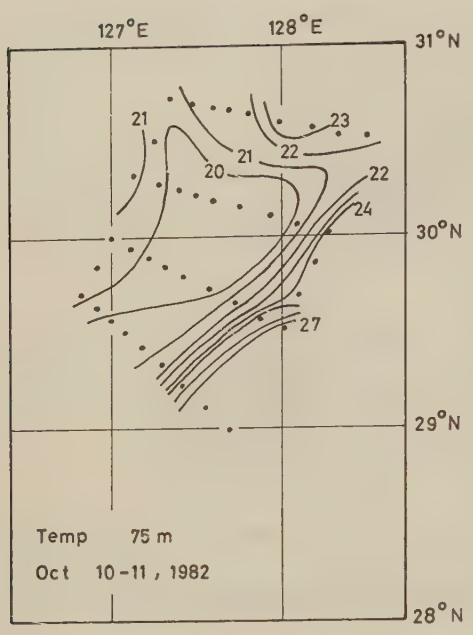

Fig. 9

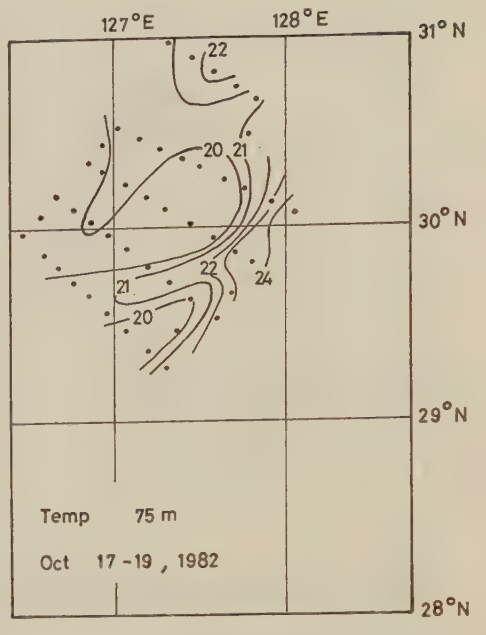

Fig. 10

Fig. 9. Water temperature onserved in the first survey in October. Depth is 75 meters. Low temperature zone sandwiched between the Kuroshio and shelf waters is noticed.

Fig. 10. Water temperature observed in the second survey in October. Depth is 75 meters.

to ascend with cyclonic rotation. These frontal eddies have folded wave patterns as seen in Figs. 2 and 4. This folding structure as shown in the figures appears to be related with effective mixing of the shelf and Kuroshio waters. The relationship between the eddies and mixing processes would be more understood, if the development of the eddy could be accurately traced.

The meander of the Kuroshio takes different paths in short intervals as observed in both surveys in May and October. Hence a rapid survey will be needed to understand the meander of the Kuroshio.

The mechanism of generation of the eddies is uncertain. As Tsujita and Kondo (1957) conjectured, the shear instability across the Kuroshio boundary may be one cause of the frontal eddies. On the other hand, since the southern eddy observed in the first survey and the eddy observed in the second survey were located at 30–50 miles downstream from the bumps mentioned in Observations, the bottom effect may be another cause of the frontal eddies. For understanding the mechanism of eddy generation we should wait for more detailed surveys made by multi-research vessels.

Acknowledgements

The authors wish to thank Captain Amemiya of the R.V. Chofu Maru and his crews for aid in field operations, and members of Oceanographical Division of the Nagasaki Marine Observatory for their co-operations in the surveys. Special acknowledgments are given to I. Fujiwara and T. Sagi for their efforts in the preparation of the survey plans and two reviewers for their helpful review comments.

References

AKIYAMA, M., K. MIYADI and Y. SUGIMORI (1982): Determination of the meso-scale eddies in the East China Sea using the thermal maps of satellite NOAA-6. Sora to Umi (The society of Airborne & Satellite Fisheries Oceanography), **5**, 11–27. (in Japanese)

JMA (1968 and 1974): the Results of Marine Meteorological and Oceanographical Observations, no. **44** and **56**.

LEE, T. N., L. P. ATKINSON and R. LEGECKIS (1981): Observations of a Gulf Stream frontal eddy on the Georgia continental shelf, April 1977. Deep-Sea Research, **28A**, 347–378.

SAWARA, T. and Y. HANZAWA (1979): Distribution of water type in the East China Sea. Umi to Sora, **54**(4), 135–148. (in Japanese)

SHIBATA, A. (1983): Meander of the Kuroshio along the edge of the continental shelf in the East China Sea. Umi to Sora, **58**(4), 113–120. (in Japanese)

TSUJI, T. and M. KONDO (1957): Some contributions to the ecology of themackerel and the oceanography of the fishing grounds in the East China Sea. Contributions from the Seikai Regional Fisheries Research Laboratory no. **93**. (in Japanese)

1982年の5月と10月に東シナ海で観測された前線渦

柴　田　　彰
（気象研究所）
江　口　一　平
（長崎海洋気象台）

1982年，東シナ海大陸棚外縁付近の海洋観測が長崎海洋気象台の調査船によって実施された．その5月の2回の調査によって，赤外衛星写真でみられるような低気圧性の渦の存在が確められた．渦は折りたたむ波の形を持ち，観測されたような折りたたみ構造は大陸棚水と黒潮水の効果的な混合に関連があるとみられる．渦の中では大陸棚水と黒潮水はともに低気圧性の回転をしながら上昇しているとみられる．渦は10月の調査でもみつかったが，5月のものよりも渦のスケールが小さいため，詳細な構造を記述するのは難しい．

The Oceanographical Magazine
Vol. 35, Nos, 1-2, pp. 31 to 34, March 1985

NOTE

On a free fall and retrieval method for a small CTD

Koichi NAGASAKA, Masaro SAIKI and Tadashi ANDOW
Japan Meteorological Agency

(Accepted, January 21, 1985)

1. Introduction

Recently, monitoring of sea water temperature and salinity of the upper portions of the global oceans is becoming of vital importance year by year for various purposes, in particular for better understanding of oceans' roles in the climatic changes of the atmosphere. However, even by applying modern observation techniques including those of satellites nothing but sea surface temperature is measured so densely and frequently almost all over the world to make analysis on ten-day/monthly basis. The efforts to expand the network of monitoring of subsurface oceanographic structure are urgently required.

For the time being, X-BT is a unique and excellent instrument to observe subsurface temperature from a cruising vessel and has advantages of ease in handling and high reliability of measurements. In the North Pacific Ocean a large amount of subsurface temperature data have been successfully obtained by using X-BTs on board merchant ships since the middle of the 1970s. Only a serious problem of using X-BTs for ocean monitoring is that expendable probes are fairly high in cost. In order to overcome this concern and to make cost-effective collection of oceanographic data in the upper few hundred meters layer of oceans, we attempted at free falling and retrieving of a small CTD probe of self data store type on board a ship under way. In the present note authors would like to describe briefly the method developed and preliminary results of tests at seas.

2. The apparatus

In developing a free fall and retrieval method, it is intended that an apparatus is capable of profiling subsurface oceanographic structure to depths up to 200 meters deep on board a ship cruising at speed up to 10 knots within 10 minutes. The feature of the apparatus is a plastic reel mounted on the top of the housing of a small CTD probe with a thin 200 meters long nylon rope as illustrated in Fig. 1. The rope is of double weaving type with diameter of 1.5 m/m and the breaking strength is rated at 90 kgf. The reel is installed inside a plastic cover to reduce drag force of water during falling and recovering. Another 300 meters long rope extended from the probe unit is stored on a drum of a shipboard winch driven by a 1/2 H.P. motor.

Upon launching the probe, the rope begins to spool off from the both of the reel and the

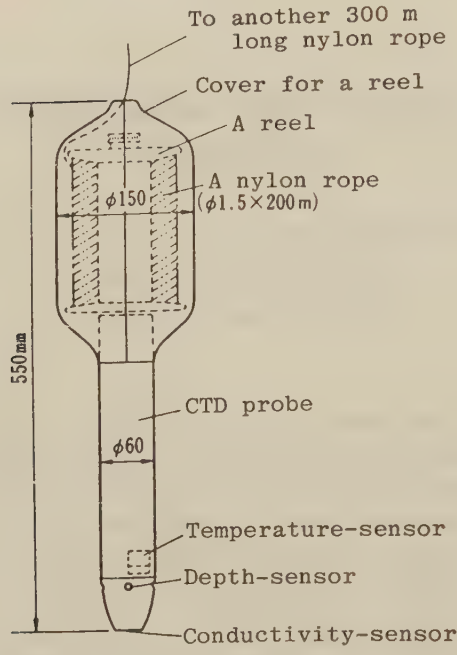

Fig. 1. A reel mounted to the pressure-tight housing of a small CTD probe for free fall.

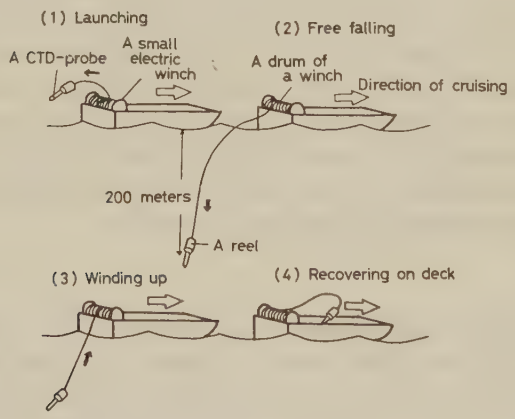

Fig. 2. Functions from launching to recovering of the probe.

drum as sinking of the profiler and cruising of the ship. Thus, the paying out of the rope from the two sides assures free fall of the probe, like X-BTs. After profiling to depths up to 200 meters, the unit is recovered by winding up the whole length of the rope on the rope on the drum. (see Fig. 2). For preparation of the next measurements, a part (200 meter long) of the rope on the drum is transferred to the reel by using an attachment to the winch.

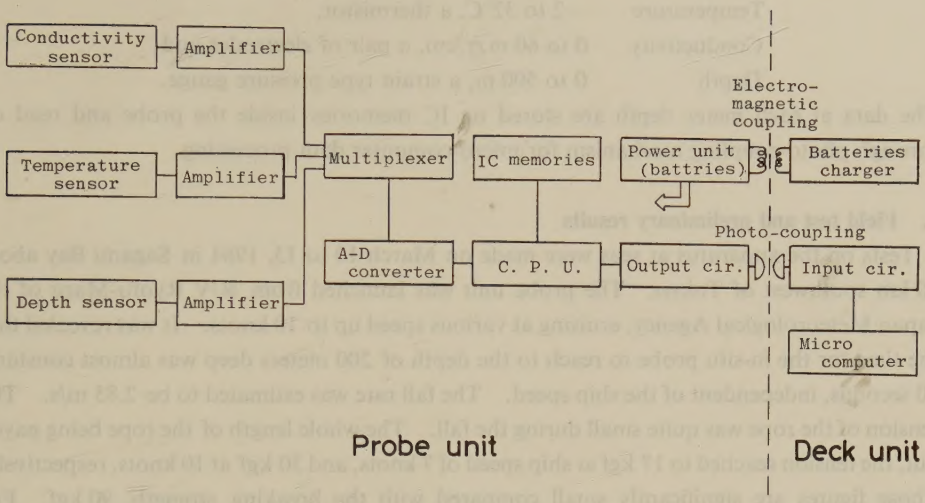

Fig. 3. A total schematic diagram of a CTD probe and a shipboard unit to read off the data stored on IC memories within the probe.

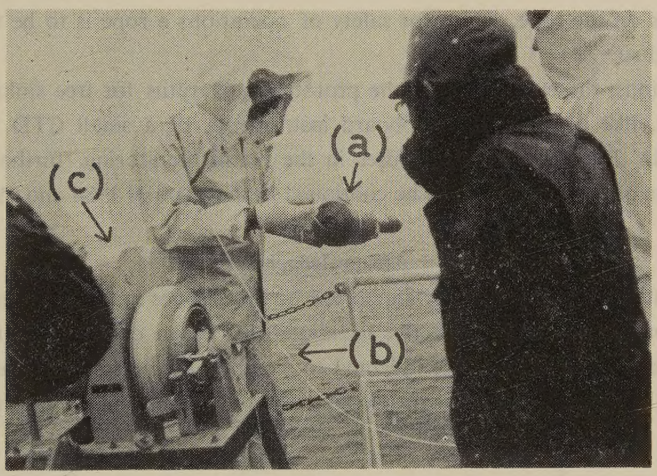

Photo. A view of field experiments on board R/V Ryofu-Maru.
(a) A probe unit with a reel for free fall
(b) A thin nylon rope, and
(c) A small winch.

Although it is out of the scope of the present note to describe details on the CTD probe and data processing, a total schematic diagram is given in Fig. 3. The dimension of the present miniature CTD manufactured by the Tsurumi Seiki CO., LTD. is only 6 cm diameter by 35 cm long without the reel, and it weighs 2.5 kg in air and 2.0 kg in water, respectively. The ranges of measurements and sensor elements are as follows;

Temperature	−2 to 32°C, a thermistor,
Conductivity	0 to 60 m℧/cm, a pair of electrodes and
Depth	0 to 500 m, a strain type pressure gauge.

The data at each meter depth are stored on IC memories inside the probe and read off through photo-coupling mechanism for micro-computer data processing.

3. Field test and preliminary results

Tests on the apparatus at seas were made on March 10 to 13, 1984 in Sagami Bay about 50 km southwest of Tokyo. The probe unit was launched from R/V Ryofu-Maru of the Japan Meteorological Agency, cruising at various speed up to 10 knots. It was revealed that the time for the in-situ probe to reach to the depth of 200 meters deep was almost constant, 70 seconds, independent of the ship speed. The fall rate was estimated to be 2.85 m/s. The tension of the rope was quite small during the fall. The whole length of the rope being payed out, the tension reached to 17 kgf at ship speed of 7 knots, and 30 kgf at 10 knots, respectively. Those figures are significantly small compared with the breaking strength, 90 kgf. For recovering of the probe unit it took 7 to 8 minutes and the rate of winding up was about 1.0 m/s.

It was found that reversing of the folds on the reel was needed every dropping in order to prevent kinks on the rope. Also for safety of operations a rope is to be renewed every 5 profilings and so.

In conclusions, the evaluations of the prototype apparatus for free sinking, like X-BTs, and retrieval, like conventional shipboard instruments, of a small CTD were fairly well accomplished. For the operational uses in the ocean monitoring, further field-tests and improvements of the devices are to be continued in the years of 1984 and 1985.

Acknowledgements

The present work was financially supported by the Science and Technology Agency as a part of the project to develop effective techniques for ocean observations in the economic zones of Japan. The authors are indebted to members of the scientific party, officers and crew aboard R/V Ryofu-Maru for their cooperation during the field experiments.

超小型 CTD プローブの投下・回収方法について

長坂昂一・佐伯理郎・安藤　正
（気象庁）

海洋表層の水温・塩分の鉛直分布の観測を航走中の船上で簡便かつ経済的に行うために，超小型 CTD プローブの投下・回収方法を開発した．プローブを自由落下させるためにプローブから落下速度に応じて，また船上のウインチドラム（回収機能も兼ねる）から船速に対応して細いナイロンロープを繰り出す機構を試作した．船速10ノットまでの船からのプローブの降下（200 m 深まで）・回収試験を行い，ほぼ良好な結果を得た．

昭和60年3月30日　発行

編集兼
発行者　気　象　庁
東京都千代田区大手町1の3の4

印刷者　青　木　俊　夫

印刷所　昌美印刷株式会社
東京都千代田区飯田橋2の6の1